Geochemistry Geophysics Geosystems G3

Published by AGU and the Geochemical Society

*Article*
Volume 13, Number 10
18 October 2012
Q10012, doi:10.1029/2012GC004332
ISSN: 1525-2027

# Seismic structure and lithospheric rheology from deep crustal xenoliths, central Montana, USA

**K. H. Mahan**
*Department of Geological Sciences, University of Colorado Boulder, Boulder, Colorado 80309, USA (mahank@colorado.edu)*

**V. Schulte-Pelkum**
*Department of Geological Sciences and Cooperative Institute for Research in Environmental Sciences, University of Colorado Boulder, Boulder, Colorado 80309, USA*

**T. J. Blackburn, S. A. Bowring, and F. O. Dudas**
*Department of Earth, Atmospheric, and Planetary Sciences, Massachusetts Institute of Technology, Cambridge, Massachusetts 02139, USA*

[1] Improved resolution of lower crustal structure, composition, and physical properties enhances our understanding and ability to model tectonic processes. The cratonic core of Montana and Wyoming, USA, contains some of the most enigmatic lower crust known in North America, with a high seismic velocity layer contributing to as much as half of the crustal column. Petrological and physical property data for xenoliths in Eocene volcanic rocks from central Montana provide new insight into the nature of the lower crust in this region. Inherent heterogeneity in xenoliths derived from depths below ~30 km support a composite origin for the deep layer. Possible intralayer velocity steps may complicate the seismic definition of the crust/mantle boundary and interpretations of crustal thickness, particularly when metasomatized upper mantle is considered. Mafic mineral-dominant crustal xenoliths and published descriptions of mica-bearing peridotite and pyroxenite xenoliths suggest a strong lower crust overlying a potentially weaker upper mantle.

**Components:** 7100 words, 2 figures, 2 tables.

**Keywords:** Montana; granulites; lower crust; seismic velocity; xenoliths.

**Index Terms:** 5102 Physical Properties of Rocks: Acoustic properties; 7205 Seismology: Continental crust (1219); 8159 Tectonophysics: Rheology: crust and lithosphere (8031).

**Received** 5 July 2012; **Revised** 7 September 2012; **Accepted** 13 September 2012; **Published** 18 October 2012.

Mahan, K. H., V. Schulte-Pelkum, T. J. Blackburn, S. A. Bowring, and F. O. Dudas (2012), Seismic structure and lithospheric rheology from deep crustal xenoliths, central Montana, USA, *Geochem. Geophys. Geosyst.*, *13*, Q10012, doi:10.1029/2012GC004332.

## 1. Introduction

[2] The Rocky Mountain and High Plains region of Montana and Wyoming, USA, (Figure 1) contain perhaps some of the most enigmatic lower crust in North America. The region is part of the cratonic core of the continent but contains a high seismic velocity lower crustal layer (>7.0 km/s P wave speed [*Gorman et al.*, 2002]) that is more than three times the mean thickness of comparable layers in Precambrian shields worldwide [*Barnhart et al.*, 2012; *Christensen and Mooney*, 1995]. This "7.x layer" averages 25 km in thickness in a crustal column that totals 49–60 km [*Gorman et al.*, 2002;

*Schutt et al.*, 2008; *Snelson et al.*, 1998], and could have had a profound influence on the rheology of the lithosphere during orogenic events subsequent to its Archean and Proterozoic construction. This paper summarizes new and existing data from crustal xenoliths in Montana that bear on the composition and physical and rheological properties of the lower crust in the region.

## 2. Background and Xenolith Data From Great Falls Tectonic Zone

[3] Montana and Wyoming consist of Archean cratons amalgamated in the Proterozoic and accreted Proterozoic terranes, both of which have been covered by Phanerozoic sedimentary rocks and Late Mesozoic and Cenozoic volcanic rocks (Figure 1). The cratons include the Medicine Hat Block to the north, which is obscured by the Western Canada Sedimentary Basin and which has been studied exclusively by geophysical methods, xenoliths, and drill core samples [e.g., *Ross*, 2002]. Basement rocks of the Wyoming craton are observed in discrete Laramide-age uplifts and through xenolith studies. The Wyoming craton and Medicine Hat Block are sutured together by the ca. 1.86–1.71 Ga Great Falls Tectonic Zone [*Giletti*, 1966; *Harms et al.*, 2004; *Mueller et al.*, 2002; *O'Neill and Lopez*, 1985]. The ca. 1.78–1.75 Ga Cheyenne Belt [*Duebendorfer et al.*, 2006; *Karlstrom and Houston*, 1984] bounds the Wyoming craton to the south, and both cratonic blocks are bounded to the east by the ca. 1.83–1.72 Ga Trans-Hudson orogen [*Bickford et al.*, 1990; *Dahl et al.*, 1999; *Maxeiner et al.*, 2005]. Crustal thickness estimates in Montana and Wyoming vary from 40 to 60 km, with much of the region underlain by a layer of anomalously thick (10–30 km) and seismically fast lower crust referred to here as the 7.x layer [*Bensen et al.*, 2009; *Gilbert*, 2012; *Gorman et al.*, 2002; *Rumpfhuber and Keller*, 2009; *Schutt et al.*, 2008; *Snelson et al.*, 1998; *Stachnik et al.*, 2008; *Yuan et al.*, 2010].

[4] Both cratonic blocks and the Great Falls Tectonic Zone contain volcanic rocks and kimberlites of the Paleogene Montana alkali igneous province [e.g., *Marvin et al.*, 1980], many localities of which contain upper mantle and lower crustal xenoliths [*Barnhart et al.*, 2012; *Blackburn et al.*, 2011, 2012a, 2012b; *Bolhar et al.*, 2007; *Buhlmann et al.*, 2000; *Carlson and Irving*, 1994; *Collerson et al.*, 1989; *Davis et al.*, 1995; *Downes et al.*, 2004; *Facer et al.*, 2009; *Hearn*, 1989; *Hearn et al.*, 1989; *Joswiak*, 1992]. Crustal xenoliths for which new data are presented here are from the Sweet Grass Hills near the Montana/Alberta border and the Homestead kimberlite in central Montana (Figure 1). The former are dated at ca. 50 Ma [e.g., *Buhlmann et al.*, 2000] and the latter are assumed to have a similar 50 Ma age based on dates from nearby kimberlite pipes in central Montana [*Hearn*, 2004].

[5] A variety of geochronological data have been reported from previous xenolith studies in the region, yielding U-Pb zircon dates ranging from late Archean (ca. 3.0 Ga) to Mesoproterozoic (ca. 1.3 Ga). Despite zircon data from a wide range of lithologies, Archean dates are reported primarily from felsic to intermediate composition mid-crustal xenoliths [*Blackburn et al.*, 2011; *Bolhar et al.*, 2007; *Davis et al.*, 1995], including one of the Sweet Grass Hills xenoliths for which seismic data are reported here (05SG-02). All published Montana xenolith studies that we are familiar with include significant if not exclusive ca. 1.8–1.7 Ga populations of dominantly metamorphic zircon and monazite [*Barnhart et al.*, 2012; *Blackburn et al.*, 2011, 2012a; *Bolhar et al.*, 2007; *Carlson and Irving*, 1994; *Davis et al.*, 1995; *Scherer et al.*, 2000], suggesting that this represents the age range of major granulite-facies metamorphism of lower crust in the region. Xenoliths from several localities in the Bears Paw Mountains volcanic field (Figure 1) contain ca. 2.2–2.1 and/or 1.4–1.3 Ga zircon or monazite [*Barnhart et al.*, 2012; *Bolhar et al.*, 2007; *Scherer et al.*, 2000], indicating early or late periods, respectively, of metamorphism and/or fluid flow events and possibly new magmatic additions to the lower crust at these times [*Barnhart et al.*, 2012]. Several reports involving chemical/mineralogical studies of both the Cenozoic volcanic rocks themselves and direct observations from mantle xenoliths suggest one or more upper mantle metasomatic events across a broad region of the Montana alkali igneous province. These include studies in the Highwood Mountains [*Carlson and Irving*, 1994; *O'Brien et al.*, 1991; *O'Brien et al.*, 1995; *Rudnick et al.*, 1999], Eagle Buttes [*Carlson and Irving*, 1994], the Bears Paw mountains [*Downes et al.*, 2004; *Facer et al.*, 2009; *MacDonald et al.*, 1992], the Crazy Mountains [*Dudas et al.*, 1987], and the Milk River area of southern Alberta [*Buhlmann et al.*, 2000] which is part of the Sweet Grass Hills igneous complex (Figure 1).

## 3. New Data From Sweet Grass Hills and Homestead Xenolith Localities

[6] New seismic velocity and density data are presented for five samples from Sweet Grass Hills (05SG-02, -03, -05, -08, and -20) and two from the Homestead kimberlite (HS-1 and HS-2). Mineral

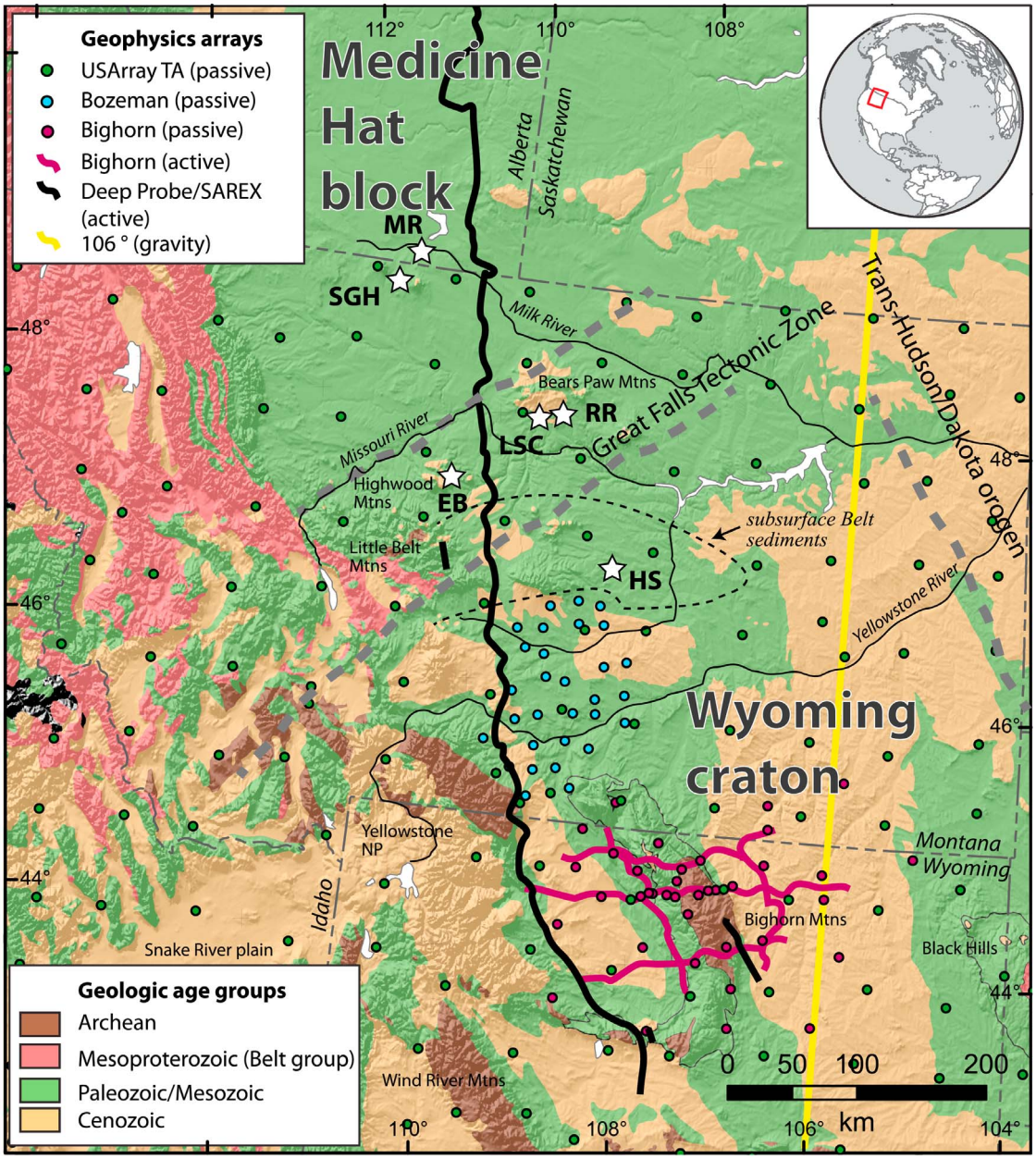


**Figure 1.** Geologic map of region centered around Montana showing xenolith localities and seismic arrays relevant to this study. Xenolith locality abbreviations: MR-Milk River, SGH-Sweet Grass Hills, RR-Robinson Ranch, LSC-Little Sand Creek, EB-Eagle Buttes, HS-Homestead. Extent of subsurface Belt basin sediments is taken from the Geologic Map of Montana [*Vuke et al.*, 2007]. Thick dashed gray lines represent approximate boundaries of the Great Falls Tectonic Zone and Trans-Hudson/Dakota orogen. The 106° gravity profile is from *Snelson et al.* [1998].

compositions and thermobarometry for three of the Sweet Grass Hills samples (05SG-02, -05, and -20) were presented by *Blackburn et al.* [2011], and data for the remaining four samples are first reported here (see auxiliary material for sample descriptions, mineral composition, photomicrographs).[1]

[7] Modal mineralogy (Table 1) was quantified by automated scanning electron microscope analysis (QEMSCAN [*Hoal et al.*, 2009; *Pirrie and Rollinson*, 2011; *Pirrie et al.*, 2004]) at the Colorado School of Mines (see auxiliary material for more information and *Pirrie and Rollinson* [2011] for a comprehensive review of the technique and modern applications). Quantitative mineral compositions (Table S1 in Text S1 the auxiliary material)

[1]Auxiliary materials are available in the HTML. doi:10.1029/2012GC004332.

**Table 1.** Modal Mineralogy for Montana Crustal Xenoliths[a]

| | Sweet Grass Hills | | | | | Homestead | | |
|---|---|---|---|---|---|---|---|---|
| | 05SG02[b] | 05SG03 | 05SG05[b] | 05SG08 | 05SG20[b] | HS1 | HS1-alt | HS2 |
| Qz | 63.94 | 8.61 | 14.31 | 0.91 | 0.00 | 0.00 | 0.00 | 0.09 |
| Grt | 9.39 | 34.51 | 25.13 | 33.83 | 55.58 | 8.57 | 2.17 | 24.69 |
| Pl | 23.95 | 23.51 | 39.58 | 26.09 | 7.77 | 36.7 | 7.31 | 52.79 |
| Cpx | 0.00 | 23.9 | 0.00 | 35.55 | 35.37 | 25.08 | 20.75 | 10.40 |
| Opx | 0.00 | 1.14 | 0.00 | 1.92 | 0.00 | 12.83 | 0.00 | 0.00 |
| Hbl | 0.00 | 0.00 | 0.00 | 0.00 | 0.00 | 13.11 | 8.78 | 6.75 |
| Sil | 0.00 | 0.00 | 1.01 | 0.00 | 0.00 | 0.00 | 0.00 | 0.00 |
| Bt | 0.45 | 0.00 | 0.92 | 0.60 | 0.00 | 0.7 | 0.7 | 0.00 |
| Kfs | 1.80 | 2.46 | 17.7 | 0.37 | 0.00 | 0.00 | 0.00 | 0.00 |
| Rt | 0.40 | 0.00 | 0.55 | 0.08 | 0.61 | 0.01 | 0.01 | 0.00 |
| Ilm[c] | 0.02 | 4.81 | 0.01 | 0.49 | 0.43 | 1.20 | 1.20 | 4.13 |
| Ap | <0.01 | 0.48 | 0.05 | 0.11 | 0.12 | 1.41 | 1.41 | 1.03 |
| Ttn | 0.00 | <0.01 | 0.00 | <0.01 | 0.00 | 0.17 | 0.17 | 0.12 |
| mag/hem | 0.00 | 0.41 | 0.56 | 0.00 | 0.00 | 0.00 | 0.00 | 0.00 |
| alteration[d] | 0.00 | 0.00 | 0.00 | 0.00 | 0.00 | 0.00 | 57.28 | 0.00 |
| Other accessories | 0.05 | 0.17 | 0.18 | 0.04 | 0.12 | 0.22 | 0.22 | <0.01 |
| Total | 100.00 | 100.00 | 100.00 | 99.99 | 100.00 | ##### | 100.00 | 100.00 |

[a]Other accessories include sulfides, monazite, zircon, etc.
[b]Modal compositions for samples 05SG02, 05SG05, and 05SG20 were reported in the appendix of *Blackburn et al.* [2011] but are included in tabulated form here for completeness.
[c]Includes both primary ilmenite and secondary ilmenite rims on rutile.
[d]Secondary alteration is minor in most samples and not included. The one exception is HS1 where >50% of the sample is altered to chlorite (~19%), albite (~16%), carbonate (~13%), actinolite (~9%), and secondary apatite and titanite.

were determined by electron microprobe at the University of Colorado Boulder. Specific analytical settings, instrumentation, and evaluation strategies are given in the auxiliary material and by *Barnhart et al.* [2012]. Bulk major element compositions were calculated from modal proportions and major and minor mineral compositions (Table S2). Following *Barnhart et al.* [2012], the samples are divided into mafic (<52 wt% $SiO_2$), intermediate (>52 wt% and <57 wt% $SiO_2$), and felsic (>57 wt% $SiO_2$) granulites (Figures 2a–2d). Of the new samples presented here, three of the Sweet Grass Hills samples (05SG-03, -08 and -20) and both Homestead xenoliths are mafic granulites. The remaining two Sweet Grass Hills samples are felsic granulites (05SG-02 and -05).

[8] Calculated pressures for two new Sweet Grass Hills samples and two Homestead samples range from 1.10 to 1.34 GPa (see auxiliary material for thermobarometry details), which falls within a broader range of pressures from 0.6 to 1.53 GPa reported for thirteen other xenoliths from central Montana reported by *Barnhart et al.* [2012]. These pressures are interpreted to approximate the depths from which the samples were derived during exhumation based on 1) the common occurrence of mineral chemical zoning characteristics that are consistent with isobaric cooling at depth for samples that lack tectonic decompression textures, 2) the presence of reaction textures in some xenoliths studied by *Barnhart et al.* [2012] that reflect post-peak tectonic decompression (in these instances, retrograde pressures were used for residence depths), and 3) the observation that all crustal xenolith localities discussed here also host mantle peridotite xenoliths. The resulting pressures correspond to ~23 to ~54 km depths using the model crustal density profile of *Christensen and Mooney* [1995].

[9] Bulk seismic properties and densities (Table 2 and Figure 2) were calculated from the modal proportions, mineral compositions, and single crystal elastic data via the physical properties spreadsheet of *Hacker and Abers* [2004]. Calculations were made at 25°C for comparison with laboratory measurements commonly reported at room temperature and at 500°C (Figures 2a–2d), which is a maximum long-term residence temperature for modern lower crust in this region [*Blackburn et al.*, 2012a], for better comparison to modern seismic observations. The Voigt-Reuss-Hill (VRH) and Hashin-Shtrikman (H-S) averages are reported in Table 2. The former [*Hill*, 1952], which is the most commonly used in Earth science literature (also used in Figure 2), is a reliable scheme for evaluating elastic properties but does not account for the geometric arrangement of mineral grains [e.g., *Mainprice and Humbert*, 1994], whereas

the latter explicitly assumes a statistically random structure [*Bunge et al.*, 2000].

## 4. Discussion

### 4.1. A Composite 7.x Layer

[10] New data from this study combined with that from *Barnhart et al.* [2012] provide a robust data set with which to evaluate the evolution, seismic structure, and rheology of the deep crust in Montana. Calculated pressures of 0.6 to 1.5+ GPa are consistent with derivation from depths of 23–54 km, and when compared to the vertical extent of the seismically defined 7.x layer [*Gorman et al.*, 2002], those from below ~32 km can likely be considered samples from within the bulk high velocity lower crustal layer (Figure 2). However, heterogeneity across a wide range of characteristics (mineralogy, textures, bulk chemical compositions,

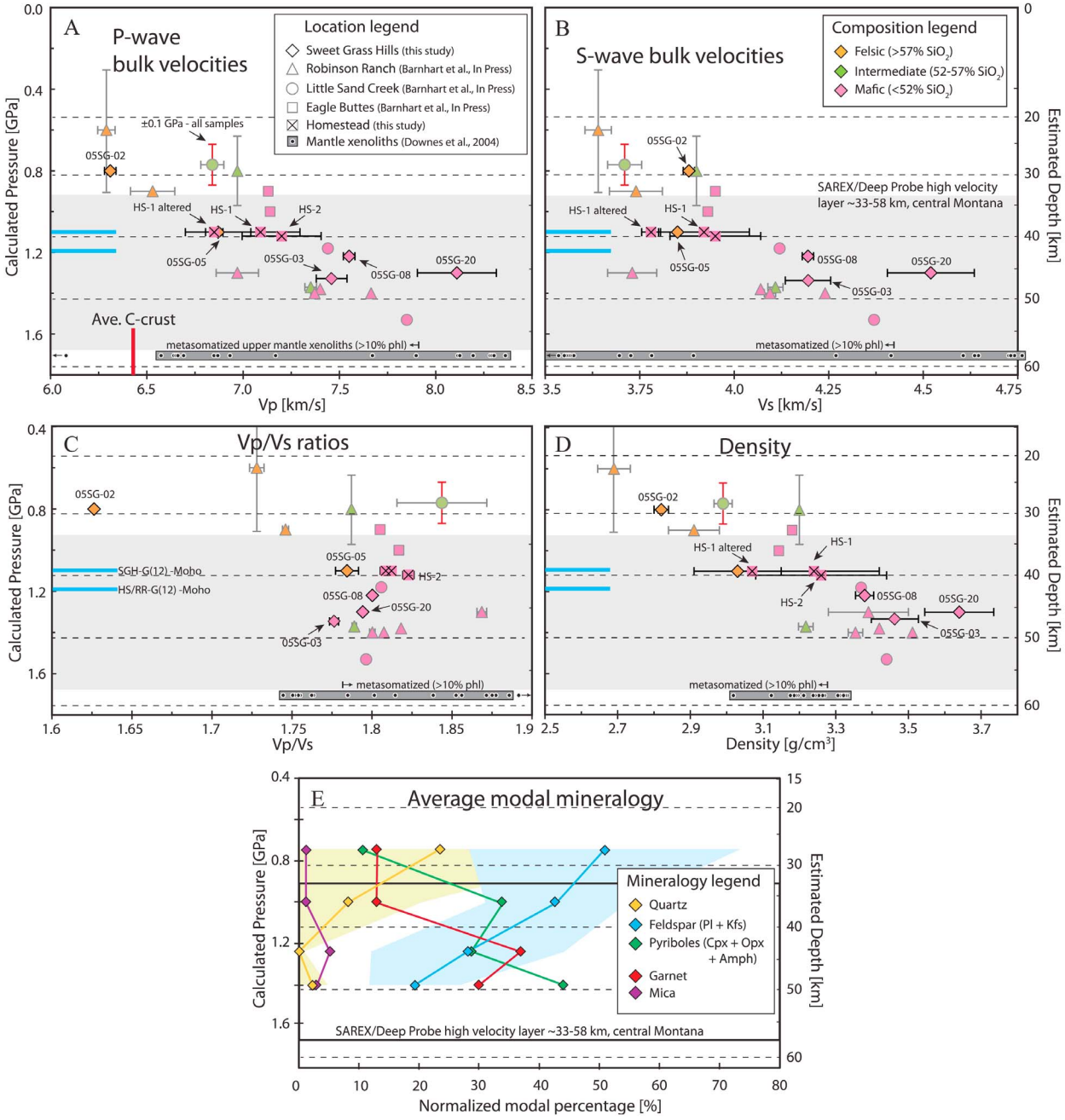


**Figure 2**

**Table 2.** Seismic Properties and Density for Montana Crustal Xenoliths[a]

| | Sweet Grass Hills | | | | | | | | | | Homestead | | | | | |
|---|---|---|---|---|---|---|---|---|---|---|---|---|---|---|---|---|
| | 05SG02 | ± | 05SG03 | ± | 05SG05 | ± | 05SG08 | ± | 05SG20 | ± | HS1 | ±[b] | HS1-alt | ± | HS2 | ± |
| P (Gpa) | 0.80 | | 1.34 | | 1.10 | | 1.21 | | 1.30 | | 1.10 | | 1.10 | | 1.12 | |
| $T_{eq}$ (°C) | 900 | | 900 | | 900 | | 855 | | 890 | | 780 | | 500 | | 785 | |
| | | | | | | | *25°C* | | | | | | | | | |
| rho (g/cm$^3$) | 2.83 | 0.02 | 3.50 | 0.07 | 3.06 | 0.12 | 3.42 | 0.03 | 3.68 | 0.10 | 3.28 | 0.19 | 3.11 | 0.01 | 3.29 | 0.19 |
| Vp (km/s) H-S | 6.40 | 0.02 | 7.55 | 0.09 | 6.95 | 0.17 | 7.72 | 0.02 | 8.28 | 0.20 | 7.26 | 0.22 | 7.00 | 0.05 | 7.33 | 0.22 |
| Vs (km/s) H-S | 4.01 | 0.02 | 4.30 | 0.06 | 3.96 | 0.08 | 4.34 | 0.01 | 4.65 | 0.11 | 4.07 | 0.13 | 3.91 | 0.03 | 4.08 | 0.13 |
| Vp/Vs H-S | 1.60 | 0.00 | 1.76 | 0.00 | 1.76 | 0.01 | 1.78 | 0.00 | 1.78 | 0.00 | 1.78 | 0.00 | 1.79 | 0.00 | 1.80 | 0.00 |
| Vp (km/s) VRH | 6.45 | 0.03 | 7.56 | 0.09 | 7.02 | 0.18 | 7.74 | 0.03 | 8.29 | 0.21 | 7.28 | 0.22 | 7.02 | 0.05 | 7.37 | 0.22 |
| Vs (km/s) VRH | 4.02 | 0.02 | 4.29 | 0.06 | 3.98 | 0.09 | 4.34 | 0.01 | 4.64 | 0.12 | 4.07 | 0.12 | 3.91 | 0.03 | 4.09 | 0.12 |
| Vp/Vs VRH | 1.60 | 0.00 | 1.76 | 0.00 | 1.76 | 0.01 | 1.78 | 0.00 | 1.79 | 0.00 | 1.79 | 0.00 | 1.80 | 0.00 | 1.80 | 0.00 |
| | | | | | | | *500°C* | | | | | | | | | |
| rho (g/cm$^3$) | 2.82 | 0.02 | 3.46 | 0.07 | 3.03 | 0.12 | 3.38 | 0.03 | 3.64 | 0.10 | 3.24 | 0.18 | 3.07 | 0.01 | 3.26 | 0.18 |
| Vp (km/s) H-S | 6.26 | 0.02 | 7.37 | 0.09 | 6.79 | 0.17 | 7.53 | 0.03 | 8.10 | 0.20 | 7.07 | 0.21 | 6.83 | 0.04 | 7.16 | 0.21 |
| Vs (km/s) H-S | 3.87 | 0.02 | 4.16 | 0.06 | 3.83 | 0.08 | 4.20 | 0.01 | 4.52 | 0.11 | 3.92 | 0.13 | 3.78 | 0.02 | 3.95 | 0.13 |
| Vp/Vs H-S | 1.62 | 0.00 | 1.77 | 0.00 | 1.77 | 0.01 | 1.79 | 0.00 | 1.79 | 0.00 | 1.80 | 0.01 | 1.81 | 0.00 | 1.81 | 0.01 |
| Vp (km/s) VRH | 6.31 | 0.03 | 7.38 | 0.09 | 6.87 | 0.17 | 7.56 | 0.03 | 8.11 | 0.21 | 7.09 | 0.21 | 6.85 | 0.04 | 7.20 | 0.21 |
| Vs (km/s) VRH | 3.88 | 0.01 | 4.15 | 0.06 | 3.85 | 0.08 | 4.20 | 0.01 | 4.52 | 0.12 | 3.92 | 0.12 | 3.78 | 0.02 | 3.95 | 0.12 |
| Vp/Vs VRH | 1.63 | 0.00 | 1.78 | 0.00 | 1.78 | 0.01 | 1.80 | 0.00 | 1.79 | 0.00 | 1.81 | 0.00 | 1.81 | 0.00 | 1.82 | 0.00 |
| | | | | | | | *$T_{eq}$* | | | | | | | | | |
| rho (g/cm$^3$) | 2.80 | 0.01 | 3.42 | 0.07 | 3.01 | 0.12 | 3.35 | 0.02 | 3.60 | 0.10 | 3.21 | 0.19 | - | - | 3.23 | 0.19 |
| Vp (km/s) H-S | 6.12 | 0.02 | 7.19 | 0.09 | 6.64 | 0.16 | 7.37 | 0.03 | 7.92 | 0.20 | 6.94 | 0.20 | - | - | 7.04 | 0.20 |
| Vs (km/s) H-S | 3.74 | 0.01 | 4.02 | 0.06 | 3.70 | 0.07 | 4.08 | 0.01 | 4.40 | 0.12 | 3.82 | 0.13 | - | - | 3.85 | 0.13 |
| Vp/Vs H-S | 1.64 | 0.00 | 1.79 | 0.00 | 1.79 | 0.01 | 1.81 | 0.00 | 1.80 | 0.00 | 1.82 | 0.01 | - | - | 1.83 | 0.01 |
| Vp (km/s) VRH | 6.17 | 0.03 | 7.20 | 0.09 | 6.72 | 0.16 | 7.40 | 0.03 | 7.93 | 0.20 | 6.96 | 0.20 | - | - | 7.08 | 0.20 |
| Vs (km/s) VRH | 3.74 | 0.02 | 4.01 | 0.06 | 3.73 | 0.07 | 4.08 | 0.01 | 4.39 | 0.12 | 3.82 | 0.12 | - | - | 3.86 | 0.12 |
| Vp/Vs VRH | 1.65 | 0.00 | 1.80 | 0.01 | 1.80 | 0.01 | 1.81 | 0.00 | 1.81 | 0.00 | 1.82 | 0.00 | - | - | 1.83 | 0.00 |

[a]VRH = Voigt-Reuss-Hill average. H-S = Hashin-Shtrikman. Velocities were calculated at Teq as well as at 25°C for comparison with laboratory measurements commonly reported at room temperature and at 500°C, which is a maximum long-term residence temperature for modern lower crust in this region [*Blackburn et al.*, 2012].

[b]Due to poor peak assemblage preservation, uncertainties for HS1 are assigned to be equivalent to those for HS2.

**Figure 2.** Calculated bulk physical properties plotted against depth for crustal xenolith samples from Montana. (a) Bulk compressional wave velocities. (b) Bulk shear wave velocities. (c) Ratio of bulk P-wave to S-wave velocities. (d) Density. New data reported in this study are those from Sweet Grass Hills and Homestead kimberlite. Also shown are data reported by *Barnhart et al.* [2012] from Robinson Ranch, Little Sand Creek, and Eagle Buttes in north-central Montana. *Barnhart et al.* [2012] calculated bulk physical properties for the Eagle Buttes samples using compositional data provided by *Joswiak* [1992]. Error bars in physical properties (*x* axis of plots) represent variation based on thin section scale compositional heterogeneity, which was evaluated by making similar calculations over halves of the full thin sections (see *Barnhart et al.* [2012] for further discussion). Error bars in pressure (*y* axis) represent nominal ±0.1 GPa for TWQ thermobarometry [*Berman*, 1991] and, while applicable to all samples, are only shown for one sample (red bars) for clarity in the figure. Exceptions to this are two samples with relatively large errors in pressure (gray bars) that reflect additional geological uncertainty in equilibrium compositions and that are taken from *Barnhart et al.* [2012]. Velocities used in plots are Voigt-Reuss-Hill averages calculated at 500°C. The depth of the Moho and extent of the 7.x layer as determined by *Gorman et al.* [2002] are shown with gray shaded background. Moho picks from *Gilbert* [2012] for stations closest to Sweet Grass Hills (SGH), Homestead (HS) and Robinson Ranch (RR) are shown by heavy blue lines. The band of data plotted at 1.7 GPa are calculated properties for 19 upper mantle (spinel-facies) xenoliths, whose compositions and modes were reported by *Downes et al.* [2004] from two sites in the Bears Paw Mountains (Little Sand Creek and Warrick Creek; data presented in Table S2 in Text S1 in the auxiliary material). Properties for mantle xenoliths with less than and greater than 10% phlogopite (indicating substantial hydrous metasomatism) are delineated with small bar and arrow. (e) Average modal mineral (or group) content versus depth. Each data point represents average modal percentage for 4–6 samples over depth ranges equivalent to pressures of <0.8, 0.8–1.1, 1.1–1.3, and 1.3–1.6 GPa. The yellow and blue shaded regions track 1 standard deviation for quartz and feldspar.

physical properties, and geochronology) suggests the 7.x layer is a composite feature [*Barnhart et al.*, 2012]. Zircon U-Pb [*Blackburn et al.*, 2011; *Blackburn et al.*, 2012a; *Bolhar et al.*, 2007; *Davis et al.*, 1995; *Scherer et al.*, 2000] and Th-U-total Pb monazite data [*Barnhart et al.*, 2012] from crustal xenoliths across a range of localities in Montana indicate igneous, metamorphic and/or fluid flow events at >2.6 Ga, 2.2–2.0 Ga, 1.83–1.68 Ga, and 1.5–1.3 Ga. The earliest Proterozoic (2.2–2.0 Ga) and Mesoproterozoic (1.5–1.3 Ga) events likely involved rift-related intra- and/or underplating of magma. The former is indicated further by exposures of similarly aged mafic dikes and sills along both the northern [*Mueller et al.*, 2004] and southern margins of the Wyoming craton [*Cox et al.*, 2000; *Harlan et al.*, 2003; *Premo and Van Schmus*, 1989]. Mesoproterozoic continental extension is indicated by the Belt Basin rift system, which extends in the subsurface to as far east as 107.5°W in central Montana [*Vuke et al.*, 2007] (Figure 1), and widespread Mesoproterozoic mafic dikes across the Wyoming craton [*Chamberlain et al.*, 2003]. The influence of ca. 1.8–1.7 Ga orogenic events on Montana crustal xenoliths is supported by petrologic evidence for polymetamorphism associated with both crustal thickening and tectonic decompression [*Barnhart et al.*, 2012] that coincide with surface geologic records of the collisional Great Falls Tectonic Zone [*Ault et al.*, 2012; *Harms et al.*, 2004; *Mueller et al.*, 2002; *Roberts et al.*, 2002]. However, it is unclear whether a significant volume of new lower crustal material was added at this time. If so, it may have been in the form of mechanically imbricated oceanic material added during suturing [*Barnhart et al.*, 2012; *Chamberlain et al.*, 2003] or syn-collisional mafic magmatism perhaps analogous to suspected Miocene underplating in Tibet [*Grujic et al.*, 2011].

## 4.2. Velocity Structure Within the 7.x Layer and Across the Moho

[11] Calculated seismic velocities for the xenoliths generally increase with estimated depth and those below ~33 km are consistent with a similar depth for the seismically imaged top of the high velocity layer (Figure 2) in central Montana from the Deep Probe/SAREX experiments [*Gorman et al.*, 2002]. Below this estimated depth, calculated velocities at 500°C vary from 6.85 to 8.11 km/s (7.02–8.29 km/s at 25°C), consistent with the 6.9–7.8 km/s velocities modeled for the lower crustal layer in the Deep Probe/SAREX experiments. While there is considerable variation in velocities from the whole suite of deeper Montana xenoliths, the data may indicate the presence of an additional delineation above and below ~40 km (Figures 2a and 2b). Above this depth, no calculated P-velocities exceed 7.2 km/s (or 3.93 km/s for S-velocities), whereas below this depth all but one exceed 7.35 km/s (and 4.07 km/s for S-velocities).

[12] The xenolith data presented here may help to resolve some apparent discrepancies in recent seismic observations. In particular, the depth to the top and bottom of the prominent high velocity deep crustal layer, and thus thickness of the layer and crust mantle boundary depth, vary significantly between the high-resolution refraction/reflection experiments of Deep Probe and SAREX [*Clowes et al.*, 2002; *Gorman et al.*, 2002] and recent regional ambient noise surface wave [*Bensen et al.*, 2009] and receiver function [*Gilbert*, 2012] studies. The results of Deep Probe/SAREX placed the top of the 7.x layer at depths ranging from 30 to 40 km in Montana and that of the Moho at nearly 60 km ("Moho" used in reference to seismic definition of crust/mantle boundary and in context of seismic experiments). The shear wave velocity model of *Bensen et al.* [2009], from which *Gilbert* [2012] also shows a vertical cross-section for Wyoming and Montana along a profile near the Deep Probe transect, places the top of the layer closer to 20 km. This discrepancy may be largely due to parameterization constraints in the *Bensen et al.* [2009] model since they impose upper and lower crystalline layers with equal starting thicknesses. However, the Montana crustal xenolith data don't exceed 7 km/s P wave velocities above ~30 km estimated depth (Figure 2a).

[13] The more pronounced discrepancy in seismic observations lies with estimates of crustal thickness. Moho depth from Deep Probe/SAREX ranges from 49 to 60 km with estimated errors of <1.5 km (58 km in central Montana [*Gorman et al.*, 2002]). *Bensen et al.* [2009] invert surface wave data to calculate crustal thicknesses of 45–50 km for our study area. However, *Moschetti et al.* [2010, Figure 6] demonstrate that surface wave inversions have an uncertainty in Moho depth of ~10 km due to a tradeoff with lower crustal velocity. The receiver function study of *Gilbert* [2012], which used USArray TA stations across the western U.S., also shows Moho depths between 39 and 50 km in central Montana. Extracted Moho depths from *Gilbert* [2012] for stations closest to xenolith localities Homestead, Robinson Ranch/Little Sand Creek, and the Sweet Grass Hills are 43 km, 43 km, and 39 km, respectively (Figure 2), with estimated errors of ±1 km. *Gilbert* [2012] uses constant velocities (Vs = 3.8 km/s, Vp/Vs = 1.74) below 16 km depth to

migrate receiver functions; replacing his lower crustal velocities with values based on the deeper xenoliths from this study increases crustal thickness by ~2 km. *Schutt et al.* [2008] estimated crustal thicknesses of 50+ km with the Billings Array, the northern end of which is near the Homestead locality (Figure 1), with a joint inversion of surface waves and receiver function delay times which is more robust with respect to the velocity-depth tradeoff than either receiver functions or surface wave inversions alone.

[14] The xenolith data are more consistent with the greater estimates of Moho depth. As *Gilbert* [2012] notes, receiver functions are most sensitive to velocity contrasts and thus the presence of a high velocity lower crust can make the crust/mantle boundary difficult to detect. As described above, the admittedly relatively small xenolith data set presented here nonetheless indicates a possible step in calculated velocities across the ~40 km plotting depth (Figures 2a and 2b) suggesting that some receiver functions may be seeing a velocity contrast "within" the 7.x layer, particularly if the velocity contrast between the lowermost crust and mantle is small (see below). *Clowes et al.* [2002] propose a similar layering at a section of the SAREX refraction line near the Canada-U.S. border, where a 2–10 km thick layer with velocities of 7.0–7.3 km/s overlies a distinctly higher velocity layer (7.5–7.9 km/s). Such an interface would further strengthen the interpretation that the 7.x layer is a composite structure [*Barnhart et al.*, 2012].

[15] The possibility of a diminished velocity contrast across the crust/mantle boundary in Montana may be even more likely if previous suggestions of regional metasomatized upper mantle are considered [e.g., *Buhlmann et al.*, 2000; *Carlson et al.*, 2004; *Downes et al.*, 2004; *Dudas et al.*, 1987; *Facer et al.*, 2009]. Calculated properties (at 500°C and 1.7 GPa) for nineteen spinel-facies upper mantle xenoliths from the Bears Paw mountains, for which modes and mineral compositions are provided by *Downes et al.* [2004], are also shown in Figure 2 (see auxiliary material for data table). The results display a strikingly diverse range of properties, with P- and S-wave velocities from >8.3 km/s to <6.5 km/s and from >4.75 km/s to <3.5 km/s, respectively. The wide range in properties is primarily due to variation from 0 to more than 50% phlogopite, one of the primary mineralogical indicators of metasomatism. The work from these and other authors suggests that the mica was introduced into the upper mantle during at least three separate events: Proterozoic, which includes some of the mica-rich (up to 36% mica) lithologies [*Carlson and Irving*, 1994; *Downes et al.*, 2004; *Rudnick et al.*, 1999], early Tertiary prior to interaction with host magmas and perhaps related to hydration from subduction of the Farallon plate [*Downes et al.*, 2004; *O'Brien et al.*, 1991, 1995], and fractional crystallization processes associated with the magmas themselves [*Buhlmann et al.*, 2000; *Downes et al.*, 2004; *O'Brien et al.*, 1991]. While the most mica-rich lithologies are interpreted as cumulates associated with the last process and thus may represent relatively localized metasomatism, the two earlier processes, which are also thought to be responsible for mica modal occurrences of up to 36%, could represent regional modification of the uppermost mantle.

### 4.3. Implications for Rheology of Montana's Lower Crust

[16] Lithospheric strength can vary widely across tectonic settings and the nature of the lower crust, particularly its composition, can play a fundamental role in strength profiles [e.g., *Afonso and Ranalli*, 2004; *Bürgmann and Dresen*, 2008; *Rutter and Brodie*, 1992]. A quartz-dominant rheology is commonly used to approximate crustal flow strength, and a recent study across the western U.S. emphasized a correlation between bulk crustal Vp/Vs, which is particularly sensitive to the presence of quartz, and Cordilleran-wide deformation [*Lowry and Perez-Gussinye*, 2011]. However, one might expect a thick high-velocity lower crust to be relatively quartz-poor and thus somewhat stronger [*Gilbert*, 2012]. This is supported by observations from the crustal xenoliths in this study, whereby depth-averaged quartz content is less than 10% below 30 km and less than 5% below ~45 km (Figure 2e), and by the distinctly higher bulk Vp/Vs observed by *Lowry and Perez-Gussinye* [2011] beneath the Montana high plains. The xenoliths suggest that quartz and feldspar content may both decrease dramatically within the depth-range of the 7.x layer at the expense of generally increasing amounts of pyroxene (+amphibole) and garnet, which is consistent with some other examples of cratonic lower crust [e.g., *Rudnick and Fountain*, 1995]. Thus, a pyroxene-dominant lower crustal rheology may be most appropriate for much of the Montana/Wyoming region.

[17] The lateral and vertical heterogeneity of rheological properties imposed by the presence of a thick and strong lower crust in Montana and Wyoming, and its absence elsewhere in the Rockies and western Cordillera, could have significant implications

for lithospheric deformation [e.g., *Axen et al.*, 1998; *Lowry and Perez-Gussinye*, 2011]. For example, widespread lower crustal flow as proposed by early models for Laramide deformation [*Bird*, 1988] would seem less likely in the northern Rocky Mountain region. However, the boundary between distinct upper and lower crustal layers or even interfaces within the lower crustal layer might serve as convenient mechanical heterogeneities for localization of Laramide-related crustal detachment surfaces [*Erslev*, 2005]. Since much of the upper mantle in the Rocky Mountain region may also be metasomatized, the result may be that the crustal contribution to lithospheric strength in the northern Rockies and high plains could be greater than that of the upper mantle [e.g., *Afonso and Ranalli*, 2004].

## 5. Conclusions

[18] Geophysical studies, xenoliths, magmatic records, and rare exposures of once deep rocks provide fundamental perspectives with which to investigate the structure, composition, and properties of lower continental crust. Each has its own inherent biases and/or limitations, making integrated approaches crucial to further our understanding of lithospheric structure and evolution. We compared the record from crustal and upper mantle xenoliths hosted by ca. 50 Ma volcanic rocks from central Montana to seismic observations from the active source Deep Probe/SAREX experiment and several other passive source studies in the region, including those utilizing EarthScope's USArray. We emphasize a composite history for the development of the high seismic velocity lower crustal layer in the Wyoming craton and southern Medicine Hat block. The possibilities of resulting heterogeneity of physical properties within the lower crustal layer and a locally reduced contrast in properties across the crust/mantle boundary owing to upper mantle metasomatism may help explain contrasting seismic interpretations of crustal thickness in the region. Xenolith compositions indicate that the high velocity lower crust is mafic and potentially stronger than its upper mantle counterpart if metasomatic effects described from the Bears Paw Mountains are widespread.

## Acknowledgments

[19] This research was funded by NSF-EarthScope grants EAR-07464246 to KHM, EAR-1053291 to VSP and KHM, and EAR-0746205 to SAB. The authors thank S. Appleby (formerly at the Colorado School of Mines) for her service at the CSM QEMSCAN facility. Constructive reviews by Randy Keller and Hilary Downes, as well as numerous discussions with Katherine Barnhart, helped to significantly improve the manuscript and are much appreciated.

## References

Afonso, J. C., and G. Ranalli (2004), Crustal and mantle strengths in continental lithosphere: Is the jelly sandwich model obsolete?, *Tectonophysics*, *394*, 221–232, doi:10.1016/j.tecto.2004.08.006.

Ault, A. K., R. M. Flowers, and K. H. Mahan (2012), Quartz shielding of sub-20 micron zircons from radiation damage-enhanced Pb loss: An example from a granulite facies mafic dike, northwestern Wyoming craton, *Earth Planet. Sci. Lett.*, *339–340*, 57–66, doi:10.1016/j.epsl.2012.04.025.

Axen, G. J., J. Selverstone, T. Byrne, and J. M. Fletcher (1998), If the strong crust leads, will the weak crust follow?, *GSA Today*, *8*(12), 1–8.

Barnhart, K. R., K. H. Mahan, T. J. Blackburn, S. A. Bowring, and F. O. Dudas (2012), Deep crustal xenoliths from central Montana: Implications for the timing and mechanisms of high-velocity lower crust formation, *Geosphere*, in press.

Bensen, G. D., M. H. Ritzwoller, and Y. Yang (2009), A 3-D shear velocity model of the crust and uppermost mantle beneath the United States from ambient seismic noise, *Geophys. J. Int.*, *177*(3), 1177–1196, doi:10.1111/j.1365-246X.2009.04125.x.

Berman, R. G. (1991), Thermobarometry using multi-equilibrium calculations: A new technique, with petrological applications, *Can. Mineral.*, *29*, 833–855.

Bickford, M. E., K. D. Collerson, J. F. Lewry, W. R. Van Schmus, and J. R. Chiarenzelli (1990), Proterozoic collisional tectonism in the Trans-Hudson orogen, Saskatchewan, *Geology*, *18*, 14–18, doi:10.1130/0091-7613(1990)018<0014:PCTITT>2.3.CO;2.

Bird, P. (1988), Formation of the Rocky Mountains, Western United States; A continuum computer model, *Science*, *239*, 1501–1507, doi:10.1126/science.239.4847.1501.

Blackburn, T. J., S. Bowring, B. Schoene, K. H. Mahan, and F. Dudas (2011), U-Pb Thermochronology: Creating a temporal record of lithosphere thermal evolution, *Contrib. Mineral. Petrol.*, *162*(3), 479–500, doi:10.1007/s00410-011-0607-6.

Blackburn, T. J., N. Shimizu, S. A. Bowring, B. Schoene, and K. H. Mahan (2012a), Zirconium in rutile speedometry: Constraining deep lithosphere temperature-time histories over a 1000–500°C temperature range, *Earth Planet. Sci. Lett.*, *317–318*, 231–240, doi:10.1016/j.epsl.2011.11.012.

Blackburn, T. J., S. A. Bowring, J. T. Perron, K. H. Mahan, F. O. Dudas, and K. R. Barnhart (2012b), A thermal and exhumation history of continents at billion year time-scales, *Science*, *335*, 73–76, doi:10.1126/science.1213496.

Bolhar, R., B. S. Kamber, and K. D. Collerson (2007), U–Th–Pb fractionation in Archaean lower continental crust: Implications for terrestrial Pb isotope systematics, *Earth Planet. Sci. Lett.*, *254*(1–2), 127–145, doi:10.1016/j.epsl.2006.11.032.

Buhlmann, A. L., P. Cavell, R. A. Burwash, R. A. Creaser, and R. W. Luth (2000), Minette bodies and cognate mica-clinopyroxenite xenoliths from the Milk River area, southern Alberta: Records of a complex history of the northernmost part of the Archean Wyoming craton, *Can. J. Earth Sci.*, *37*, 1629–1650, doi:10.1139/e00-058.

Bunge, H. J., R. Kiewel, T. Reinert, and L. Fritsche (2000), Elastic properties of polycrystals – Influence of texture and stereology, *J. Mech. Phys. Solids*, *48*, 29–66.

Bürgmann, R., and G. Dresen (2008), Rheology of the lower crust and upper mantle: Evidence from rock mechanics, geodesy, and field observations, *Annu. Rev. Earth Planet. Sci.*, *36*, 531–567, doi:10.1146/annurev.earth.36.031207.124326.

Carlson, R. W., and A. Irving (1994), Depletion and enrichment history of subcontinental lithospheric mantle: An Os, Sr, Nd and Pb isotopic study of ultramafic xenoliths from the northwestern Wyoming Craton, *Earth Planet. Sci. Lett.*, *126*, 457–472, doi:10.1016/0012-821X(94)90124-4.

Carlson, R. W., A. J. Irving, D. J. Schulze, and B. C. Hearn Jr. (2004), Timing of Precambrian melt depletion and Phanerozoic refertilization events in the lithospheric mantle of the Wyoming Craton and adjacent Central Plains Orogen, *Lithos*, *77*, 453–472, doi:10.1016/j.lithos.2004.03.030.

Chamberlain, K. R., C. D. Frost, and R. Frost (2003), Early Archean and Mesoproterozoic evolution of the Wyoming Province: Archean origins to modern lithospheric architecture, *Can. J. Earth Sci.*, *40*, 1357–1374, doi:10.1139/e03-054.

Christensen, N. I., and W. D. Mooney (1995), Seismic velocity structure and composition of the continental crust: A global view, *J. Geophys. Res.*, *100*(B6), 9761–9788, doi:10.1029/95JB00259.

Clowes, R. M., M. J. A. Burianyk, A. R. Gorman, and E. R. Kanasewich (2002), Crustal velocity structure from SAREX, the Southern Alberta Refraction Experiment, *Can. J. Earth Sci.*, *39*, 351–373, doi:10.1139/e01-070.

Collerson, K., B. C. Hearn, R. A. MacDonald, B. G. J. Upton, and R. S. Harmon (1989), Composition and evolution of lower continental crust: Evidence from xenoliths in Eocene lavas from the Bearpaw Mountains, Montana, *N. M. Bur. Mines Resour. Bull.*, *131*, 57.

Cox, D. M., C. D. Frost, and K. R. Chamberlain (2000), 2.01-Ga Kennedy dike swarm, southeastern Wyoming: Record of a rifted margin along the southern Wyoming province, *Rocky Mt. Geol.*, *35*, 7–30, doi:10.2113/35.1.7.

Dahl, P. S., D. K. Holm, E. T. Gardner, F. A. Hubacher, and K. A. Foland (1999), New constraints on the timing of Early Proterozoic tectonism in the Black Hills (South Dakota), with implications for docking of the Wyoming province with Laurentia, *Geol. Soc. Am. Bull.*, *111*(9), 1335–1349, doi:10.1130/0016-7606(1999)111<1335:NCOTTO>2.3.CO;2.

Davis, W. J., R. G. Berman, and B. Kjarsgaard (1995), U-Pb geochronology and isotopic studies of crustal xenoliths from the Archean Medicine Hat Block, northern Montana, paper presented at Alberta Basement Transects; Report of the Transect Workshop, Univ. of B. C., Calgary, Alberta, Canada.

Downes, H., R. MacDonald, B. G. J. Upton, K. G. Cox, J. Bodinier, P. R. D. Mason, D. James, P. G. Hill, and B. C. Hearn Jr. (2004), Ultramafic xenoliths from the Bearpaw Mountains, Montana, USA: Evidence for multiple metasomatic events in the lithospheric mantle beneath the Wyoming craton, *J. Petrol.*, *45*(8), 1631–1662, doi:10.1093/petrology/egh027.

Dudas, F. O., R. W. Carlson, and D. H. Eggler (1987), Regional Middle Proterozoic enrichment of the subcontinental mantle source of igneous rocks from central Montana, *Geology*, *15*, 22–25, doi:10.1130/0091-7613(1987)15<22:RMPEOT>2.0.CO;2.

Duebendorfer, E. M., K. R. Chamberlain, and M. T. Heizler (2006), Filling the North American Proterozoic tectonic gap: 1.60–1.59 Ga deformation and orogenesis in southern Wyoming, USA, *J. Geol.*, *114*, 19–42, doi:10.1086/498098.

Erslev, E. (2005), 2D Laramide geometries and kinematics of the Rocky Mountains, Western USA, in *The Rocky Mountain Region—An Evolving Lithosphere: Tectonics, Geochemistry, and Geophysics*, *Geophys. Monogr. Ser.*, vol. 154, edited by K. E. Kalstrom and G. R. Keller, pp. 7–20, AGU, Washington, D. C., doi:10.1029/154GM02.

Facer, J., H. Downes, and A. Beard (2009), In situ serpentinization and hydrous fluid metasomatism in spinel dunite xenoliths from the Bearpaw Mountains, Montana, USA, *J. Petrol.*, *50*(8), 1443–1475, doi:10.1093/petrology/egp037.

Gilbert, H. (2012), Crustal structure of the western United States: Ancient structures overprinted by younger tectonism, *Geosphere*, *8*(1), 141–157, doi:10.1130/GES00720.1.

Giletti, B. J. (1966), Isotopic ages from southwestern Montana, *J. Geophys. Res.*, *71*, 4029–4036, doi:10.1029/JZ071i016p04029.

Gorman, A. R., et al. (2002), Deep probe: Imaging the roots of western North America, *Can. J. Earth Sci.*, *39*(3), 375–398, doi:10.1139/e01-064.

Grujic, D., C. J. Warren, and J. L. Wooden (2011), Rapid synconvergent exhumation of miocene-aged lower orogenic crust in the eastern Himalaya, *Lithosphere*, *3*(5), 346–366, doi:10.1130/L154.1.

Hacker, B., and G. Abers (2004), Subduction Factory 3: An Excel worksheet and macro for calculating the densities, seismic wave speeds, and $H_2O$ contents of minerals and rocks at pressure and temperature, *Geochem. Geophys. Geosyst.*, *5*, Q01005, doi:10.1029/2003GC000614.

Harlan, S. S., J. W. Geissman, and W. R. Premo (2003), Paleomagnetism and geochronology of and Early Proterozoic quartz diorite in the southern Wind River Range, Wyoming, USA, *Tectonophysics*, *362*, 105–122, doi:10.1016/S0040-1951(02)00633-9.

Harms, T. A., J. B. Brady, H. R. Burger, and J. T. Cheney (2004), Advances in the geology of the Tobacco Root Mountains, Montana, and their implications for the history of the northern Wyoming province, in *Precambrian Geology of the Tobacco Root Mountains, Montana*, edited by J. Brady et al., *Spec. Pap. Geol. Soc. Am.*, *377*, 227–243.

Hearn, B. C., Jr. (1989), Bearpaw Mountains, Montana, in *Montana High-Potassimn Igneous Province: Crazy Mountains to Jordan, Montana, Field Trip Guideb.*, vol. T346, pp. 51–61, AGU, Washington, D. C., doi:10.1029/FT346p0051.

Hearn, B. C., Jr. (2004), The Homestead kimberlite, central Montana, USA xenocrysts, and upper mantle xenoliths, *Lithos*, *77*, 473–491, doi:10.1016/j.lithos.2004.04.030.

Hearn, B. C., Jr., K. D. Collerson, R. A. MacDonald, and B. G. J. Upton (1989), Mantle-crustal lithosphere of north central Montana, U.S.A.: Evidence from xenoliths: Continental Magmatism, *N. M. Bur. Mines Resour. Bull.*, *131*, 125.

Hill, R. (1952), The elastic behavior of a crystalline aggregate, *Proc. Phys. Soc. London, Sect. A*, *65*, 349–354, doi:10.1088/0370-1298/65/5/307.

Hoal, K. O., S. K. Appleby, J. G. Stammer, and C. Palmer (2009), SEM-based quantitative mineralogical analysis of peridotite, kimberlite, and concentrate, *Lithosphere*, *112*, 41–46.

Joswiak, D. (1992), Composition and evolution of the lower crust, central Montana; evidence for granulite xenoliths, MSc thesis, 154 pp., Univ. of Wash., Seattle.

Karlstrom, K. E., and R. S. Houston (1984), The Cheyenne Belt: Analysis of a Proterozoic suture in southern Wyoming,

*Precambrian Res.*, *25*, 415–446, doi:10.1016/0301-9268(84)90012-3.

Lowry, A. R., and M. Perez-Gussinye (2011), The role of crustal quartz in controlling Cordilleran deformation, *Nature*, *471*, 353–357, doi:10.1038/nature09912.

MacDonald, R. A., B. G. J. Upton, K. Collerson, B. C. Hearn, and D. James (1992), Potassic mafic lavas of the Bearpaw Mountains, Montana: Mineralogy, chemistry, and origin, *J. Petrol.*, *33*(2), 305–346.

Mainprice, D., and M. Humbert (1994), Methods of calculating petrophysical properties from lattice preferred orientation data, *Surv. Geophys.*, *15*, 575–592.

Marvin, R. F., B. C. Hearn, H. H. Mehnert, C. W. Naeser, R. E. Zartman, and D. A. Lindsey (1980), Late Cretaceous-Paleocene-Eocene igneous activity in north-central Montana, *Isochron West*, *29*(3), 5–25.

Maxeiner, R. O., D. Corrigan, C. T. Harper, D. G. MacDougall, and K. Ansdell (2005), Paleoproterozoic arc and ophiolitic rocks on the northwest-margin of the Trans-Hudson Orogen, Saskatchewan, Canada: Their contribution to a revised tectonic framework for the orogen, *Precambrian Res.*, *136*, 67–106, doi:10.1016/j.precamres.2004.10.003.

Moschetti, M. P., M. H. Ritzwoller, F. C. Lin, and Y. Yang (2010), Crustal shear wave velocity structure of the western United States inferred from ambient seismic noise and earthquake data, *J. Geophys. Res.*, *115*, B10306, doi:10.1029/2010JB007448.

Mueller, P. A., A. L. Heatherington, D. M. Kelly, J. L. Wooden, and D. W. Mogk (2002), Paleoproterozioc crust within the Great Falls techtonic zone: Implications for the assembly of southern Laurentia, *Geology*, *30*, 127–130, doi:10.1130/0091-7613(2002)030<0127:PCWTGF>2.0.CO;2.

Mueller, P. A., H. R. Burger, J. L. Wooden, A. L. Heatherington, D. W. Mogk, and K. D'Arcy (2004), Age and evolution of the Precambrian crust of the Tobacco Root Mountains, in *Precambrian Geology of the Tobacco Root Mountains, Montana*, edited by J. Brady et al., *Spec. Pap. Geol. Soc. Am.*, *377*, 181–202.

O'Brien, H. E., A. J. Irving, and I. W. McCallum (1991), Eocene potassic magmatism in the Highwood Mountains, Montana: Petrology, geochemistry and tectonic implications, *J. Geophys. Res.*, *96*, 13,237–13,260, doi:10.1029/91JB00599.

O'Brien, H. E., A. J. Irving, I. W. McCallum, and M. F. Thirlwall (1995), Strontium, neodymium, and lead isotopic evidence for the interaction of post-subduction asthenospheric potassic mafic magmas of the Highwood Mountains, Montana, USA, with ancient Wyoming craton lithospheric mantle, *Geochim. Cosmochim. Acta*, *59*, 4539–4556, doi:10.1016/0016-7037(95)99266-J.

O'Neill, J., and D. Lopez (1985), Character and regional significance of Great Fall techtonic zone, east-central Idaho and west-central Montana, *Am. Assoc. Pet. Geol. Bull.*, *69*, 437–447.

Pirrie, D., and G. K. Rollinson (2011), Unlocking the applications of automated mineral analysis, *Geol. Today*, *27*, 226–235, doi:10.1111/j.1365-2451.2011.00818.x.

Pirrie, D., A. Butcher, M. Power, P. Gottlieb, and G. L. Miller (2004), Rapid quantitative mineral and phase analysis using automated scanning electron microscopy (QemSCAN); potential applications in forensic geoscience, *Geol. Soc. Spec. Publ.*, *232*, 123–136, doi:10.1144/GSL.SP.2004.232.01.12.

Premo, W. R., and W. R. Van Schmus (1989), Zircon geochronology of Precambrian rocks in southeastern Wyoming and northern Colorado, in *Proterozoic Geology of the Southern Rocky Mountains*, edited by J. A. Grambling and B. J. Tewksbury, *Spec. Pap. Geol. Soc. Am.*, *235*, 1–12.

Roberts, H., P. Dahl, S. A. Kelley, and R. Frei (2002), New $^{207}Pb/^{206}Pb$ and $^{40}Ar/^{39}Ar$ ages from SW Montana, USA: Constraints on the Proterozoic and Archean tectonic and depositional history of the Wyoming Province, *Precambrian Res.*, *117*, 119–143, doi:10.1016/S0301-9268(02)00076-1.

Ross, G. M. (2002), Evolution of Precambrian continental lithosphere in Western Canada: Results from lithoprobe studies in Alberta and beyond, *Can. J. Earth Sci.*, *39*(3), 413–437, doi:10.1139/e02-012.

Rudnick, R. L., and D. M. Fountain (1995), Nature and composition of the continental-crust: A lower crustal perspective, *Rev. Geophys.*, *33*(3), 267–309, doi:10.1029/95RG01302.

Rudnick, R. L., T. Ireland, G. E. Gehrels, A. Irving, J. Chesley, and J. M. Hanchar (1999), Dating mantle metasomatism; U-Pb geochronology of zircons in cratonic mantle xenoliths from Montana and Tanzania, in *Proceedings of the Seventh International Kimberlite Conference*, vol. 2, edited by J. J. Gurney et al., pp. 728–735, Red Roof Design, Cape Town.

Rumpfhuber, E. M., and G. R. Keller (2009), An integrated analysis of controlled and passive source seismic data across an Archean-Proterozoic suture zone in the Rocky Mountains, *J. Geophys. Res.*, *114*, B08305, doi:10.1029/2008JB005886.

Rutter, E. H., and K. H. Brodie (1992), Rheology of the lower crust, in *Continental Lower Crust*, edited by D. M. Fountain, R. Arculus, and R. W. Kay, pp. 201–267, Elsevier, Amsterdam.

Scherer, E., K. Cameron, and J. Blichert-Toft (2000), Lu–hf garnet geochronology: Closure temperature relative to the Sm–Nd system and the effects of trace mineral inclusions, *Geochim. Cosmochim. Acta*, *64*(19), 3413–3432, doi:10.1016/S0016-7037(00)00440-3.

Schutt, D. L., K. Dueker, and H. Yuan (2008), Crust and upper mantle velocity structure of the Yellowstone hot spot and surroundings, *J. Geophys. Res.*, *113*, B03310, doi:10.1029/2007JB005109.

Snelson, C. M., T. J. Henstock, G. R. Keller, K. C. Miller, and A. Levander (1998), Crustal and uppermost mantle structure along the Deep Probe seismic profile, *Rocky Mt. Geol.*, *33*(2), 181–198.

Stachnik, J. C., K. Dueker, D. L. Schutt, and H. Yuan (2008), Imaging Yellowstone plume-lithosphere interactions from inversion of ballistic and diffusive Rayleigh wave dispersion and crustal thickness data, *Geochem. Geophys. Geosyst.*, *9*, Q06004, doi:10.1029/2008GC001992.

Vuke, S. M., K. W. Porter, J. D. Lonn, and D. A. Lopez (2007), Geologic map of Montana, *Geol. Map 62*, Montana Bur. of Mines and Geol., Butte.

Yuan, H., K. Dueker, and J. Stachnik (2010), Crustal structure and thickness along the Yellowstone hot spot track: Evidence for lower crustal outflow from beneath the eastern Snake River Plain, *Geochem. Geophys. Geosyst.*, *11*, Q03009, doi:10.1029/2009GC002787.